Airborne Radar Clutter Simulation Using Hyperspectral and Lidar Imagery

Mehmet Saygın Seyfioğlu[1], Sevgi Zübeyde Gürbüz[1,2]
[1]Department of Electrical and Electronics Engineering, TOBB University of Economics and Technology, and
[2]TUBITAK Space Technologies Research Institute, Image Processing Group, Ankara, Turkey
szgurbuz@etu.edu.tr, sevgi.gurbuz@tubitak.gov.tr

***Abstract*—A key factor degrading the performance of airborne radar is clutter. Many current clutter mitigation algorithms rely on statistical clutter models; however, such models fail to incorporate the time varying, site dependent nature of unwanted scattering. Hyperspectral imagery combined with lidar-derived elevation data offers a unique and comprehensive assessment of the radar clutter environment. Elevation data can be used to compute the range of scatters to the radar, while hyperspectral data processing can yield information on terrain features, which directly impacts electromagnetic backscattering. A simulated airborne clutter map is provided, and statistics compared to typical clutter distributions.**

Keywords—radar clutter simulation, hyperspectral image classification, digital elevation model, lidar

I. INTRODUCTION

Clutter is defined as the electromagnetic backscatter from all unwanted objects residing within the footprint of the radar. The power of clutter returns is dependent upon many factors, including polarization, frequency of operation, grazing angle, and surface characteristics, such as roughness. Thus, the clutter returns are site dependent and time varying. Seasonal changes affecting the amount of leaves on trees, height of bushes and grasses, or soil moisture after rainfall all affect electromagnetic backscattering.

As a result, many target detection algorithms rely on statistical models of clutter returns to set detection thresholds, while clutter mitigation algorithms require an estimate of clutter covariance, often obtained by computing the statistics of the data in range bins neighboring the target range. However, covariance estimates can be corrupted if target backscatter spills over into neighboring bins.

Site-specific clutter maps, on the other hand, can not only be exploited to improve target detection, but can also be used to optimize radar sensor deployment, mission planning, or flight routes, and, most importantly, to provide site-specific, timely clutter information to the radar signal processor. Knowledge-based space-time adaptive processing [1] remains an active area of research focusing on using prior knowledge to improve clutter suppression.

Remote sensing data, such as optical, multi-spectral, hyperspectral, and lidar data, offer alternate sources of site-specific information that can be used to simulate clutter and thereby improve the performance of airborne radar. An example of early work is that of Garside and Oliver [2], who in 1988 showed that the texture associated with natural clutter in both optical and radar images are both consistent with a gamma-distributed correlated noise model. It was thus proposed that in the absence of true radar imagery, optical imagery could be used to simulate radar-like images.

To this aim, most work to date has utilized digital elevation models (DEM) combined with models of electromagnetic scattering from different types of terrain to simulate radar clutter [3-10]. Wang, et. al. [9] and Shasha [10] used only DEM data to compute clutter radar cross section; however, typically, some form of land use or topographical information is used in addition to DEM in these methods to capture the difference in backscattering of varying materials.

Rather than using terrain information pre-stored in databases or maps, remote sensing images can be used to provide up-to-date information on the landforms viewed by the radar. In 2011, Kurekin, et. al. [11] used multispectral LANDSAT 7+ ETM imagery together with DEM data to compensate for differences in grazing angle and convert the surface backscatter coefficients extracted from an airborne X-band radar into a simulated clutter map of a low-grazing angle land-based radar. However, it was found that roads and urban regions could not be automatically classified from the LANDSAT images; thus, man-made cultural features were extracted from topographical maps, not remote sensing data.

Hyperspectral imagery, on the other hand, offers unique advantages over multispectral data. Not only can the substances comprising a pixel be determined, but the abundance level of each substance can be estimated. Thus, hyperspectral imagery is very useful for classifying terrain type. In this work, airborne radar clutter is simulated using only remote sensing data – no topographical information from maps is utilized. The elevation data derived form lidar characterizes not just terrain shape, but also provides the height of objects, such as buildings, vehicles, and trees, which are critical to clutter modeling. A three-region clutter model that depends upon grazing angle and terrain type is employed to compute backscatter. The resultant clutter map is provided for an example airborne radar, and clutter statistics compared to typically used clutter distributions.

This work was supported by EU FP7 Project No. PIRG-GA-2010-268276 and TUBITAK Kariyer Project No. 113E105.

II. Modeling Electromagnetic Backscatter

Typical surface clutter is highly inhomogenous. The radar cross section (RCS) of a clutter patch is dependent upon a number of factors, such as resolution, grazing angle, terrain characteristics, range, frequency, polarization, and even soil moisture. One of the most ubiqutous clutter models is the constant-gamma model [12], in which the clutter reflectivity is given by

$$\sigma_0 = \frac{1}{N}\sum_{n=1}^{N}\sigma_{0,n} = \frac{1}{N}\sum_{n=1}^{N}\gamma\sin(\psi_n), \qquad (1)$$

where N is the number of known elevation points, as given from the elevation data derived from the lidar point cloud; ψ_n is the grazing angle corresponding to the n^{th} elevation point; and γ is a constant depending on terrain type and frequency.

The constant-gamma model has been shown [13] to work well in the plateau region, but exhibits significant deviations from measurements in the low and high grazing angle regions (Figure 1). The critical angle, θ_c, can be computed from the root mean square (rms) height of surface irregularities, σ_h, in wavelengths as [12]

$$\theta_c = \sin^{-1}\left(\frac{\lambda}{8\sigma_h}\right), \qquad (2)$$

where λ is the radar wavelength. For L-band radar, the critical angle is approximately 6°-7° [15]. Although aircraft typically fly at high enough an altitude that the grazing angle lies above the critical angle, low-flying unmanned aerial vehicles and helicopters may very well encounter low-angle surface clutter, for which alternate backscatter models should be used.

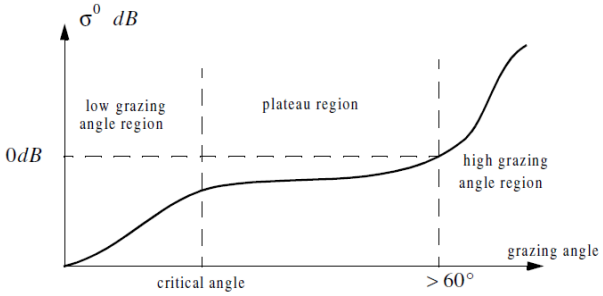

Figure 1. General dependence of clutter reflectivity on grazing angle [14].

A. Low Angle Clutter Modeling

Over the years, several different models for low-angle clutter backscatter have been put forth [4, 12, 16], among which the MIT Lincoln Laboratory Five Frequency Terrain Clutter Model (MITLL5F model, for short) is the most known. The MITLL5F model is based on extensive surface clutter measurements made over a twenty year period between the late 1970s and 1980s using radars in five different frequency bands (VHF, UHF, L, S, and X) at 42 different sites scattered about North America. From these measurements, the median value of σ_0 may be computed (Table 1) for five different terrain types: (a) desert, marsh, and grassland, (b) forest (low/high relief), (c) mountains, (d) urban, and (e) agricultural (very low/moderately low/high relief). Low relief is defined as a region where the terrain slope is less than 2°, while high relief refers to terrain slopes greater than 2°.

Table 1. Median σ_0 Values from MITLL5F Model (dB) [3]

REGION	Depression Angle (°)	VHF	UHF	L	S	X
Desert, marsh, grassland	> 1.0	-45.7	-50.8	-50.7	-42.7	-28.4
	< 0.3	-70.8	-79.6	-80.4	-59.2	-51.1
Forest/low relief	> 1.0	-21.2	-23.0	-28.0	-36.3	-34.0
	0.4 to 1.0	-32.1	-37.7	-36.9	-41.4	-38.8
	< 0.4	-54.1	-51.4	-50.5	-49.2	-44.7
Forest/ high relief	> 1.0	-16.4	-22.4	-26.5	-32.7	-28.4
	< 0.2	-29.4	-27.3	-31.1	-29.2	-34.5
Mountains	All	-23.1	-18.7	-24.3	-30.3	-28.8
Urban	All	-32.3	-31.8	-31.1	-31.0	-29.5
Agricultural, according to relief:						
High	All	-42.1	-38.9	-39.1	-47.7	-43.4
Moderately low	All	-39.1	-41.8	-43.4	-46.1	-40.0
Very low relief	All	-64.7	-54.7	-47.7	-51.2	-45.1

B. High Angle Clutter Modeling

At high grazing angles, the clutter backscatter can be approximated by the backscattering coefficient of a flat conducting surface of infinite extent [12, 15]. The flat plat approximation can also be used to approximate the scattering from calm water surfaces if the illuminated area is small and the curvature of the Earth's surface can be ignored. In this case, it can be shown that the clutter backscatter is primarily dependent upon system parameters, in particular antenna gain, as opposed to site characteristics [15]:

$$\sigma_0 = \frac{G}{4}, \qquad (3)$$

where G is the antenna gain, which for a constant transmitter power is determined by the antenna beam pattern.

III. Hyperspectral and Lidar Data Analysis

When considering the classification of hyperspectral data for the purpose of clutter modeling, the following observations should be considered:

(1) Extremely fine classification of hyperspectral imagery does not necessarily result in the optimal clutter model. If an image is over-classified, the separation between classes is reduced while the spread within a given class may remain significant. For example, in the Lincoln Lab study, initially nine different terrain classes were considered (level, inclined, undulating, rolling, hummocky, ridged, moderately steep, steep, and broken) before concluding that five classes better approximated the measurements.

(2) Terrain slope has a significant impact on clutter reflectivity; however, computing the grazing angle at each

elevation data point does not result in better match between model and measured data, primarily because the elevation data is not as precise or as accurate enough to provide terrain slope data at the scale of radar wavelengths.

Thus, in this work, grazing angle is not estimated at each individual lidar data point, but from the overall slope of regions within the image. These regions are not necessarily identical to the classification regions. For example, a large grassy area may experience significant terrain slope changes. The elevation data is clustered according to point-wise slopes; then the average slope for a cluster is used in the clutter model.

As an example, the hyperspectral imagery and lidar data of the Houston area that was provided for the 2013 IGARSS Data Fusion Contest was utilized. The hyperspectral image was classified using features extracted with Principle Component Analysis (PCA), from which 20 features were selected. An additional 3 features were computed from the Gray-level Co-occurrence Matrix (GLCM). These features were then supplied to a support vector machine and maximum likelihood classifier to obtain the final classified image, shown in Figure 2. Grassy areas were differentiated from trees using the elevation data extracted from the lidar data, so the classes of the hyperspectral imagery were mapped to the classes required by the clutter model as follows:

Road, Urban, and Roof → Urban clutter
Grass → Desert, marsh, grassland clutter
Trees → Forest (low relief – city terrain is flat)
Soil → Agricultural (very low relief – city terrain is flat)

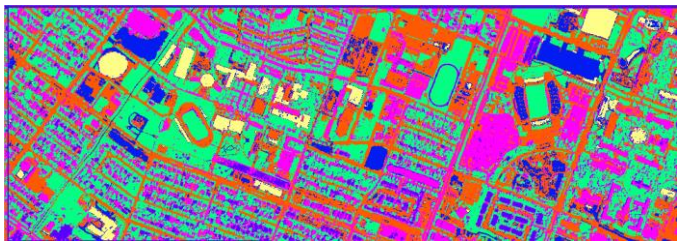

Figure 2. Classified hyperspectral image.
red: road | green: grass or tree | blue: soil | violet: urban | cream: roof

The accompanying Digital Surface Model derived from the lidar point cloud is shown in Figure 3. The lidar image is co-registered to the hyperspectral image shown in Figure 2, and gives the elevation relative to sea level in units of meters. Given the elevation and geographic coordinates of the radar, the elevation data was used to compute the range and grazing angle of each pixel to the radar, as accomplished for the specific scenario described in the Results Section.

Figure 3. Lidar image reflecting varying elevations.

III. Results

An example clutter map is generated for X-Band and VHF Band radars with an elevation beam width of 26° and azimuth beam width of 4°, numbers with are not atypical for low-flying unmanned aerial vehicles (UAV) [17-18]. The UAV is taken to be flying at an elevation of 3.7 km searching for targets about a nominal range of 3 km. This leads to a radar footprint of approximately 700 m by 340 m, which is then randomly selected from within the hyperspectral and corresponding LIDAR data. Since the resolution of the optical imagery is 2.5 meters, this footprint is comprised of 291 x 129 pixels, shown in Figure 4 and Figure 5 for the hyperspectral and lidar images, respectively.

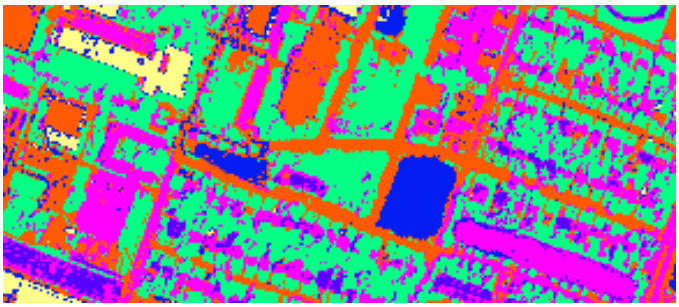

Figure 4. Sub-region of full hyperspectral image corresponding to a randomly selected radar footprint.

Figure 5. Sub-region of full lidar image corresponding to a randomly selected radar footprint.

Given the classification information and grazing angle for each pixel, the corresponding clutter reflectivity is extracted from Table 1 and used to generate the clutter map. Two example clutter maps are shown in Figure 6 and Figure 7 for X-band and VHF-band radars, respectively.

IV. Conclusion

In this work, optical imagery – in particular, hyperspectral and lidar data – was used to compute an approximation to the clutter map that would be expected to be seen by a low-flying airborne vehicle over the areas depicted in the optical imagery. In future work, such site-specific clutter information will be used to improve target detection probabilities of targets, with the aim of developing cooperative operation of optical and radar sensors.

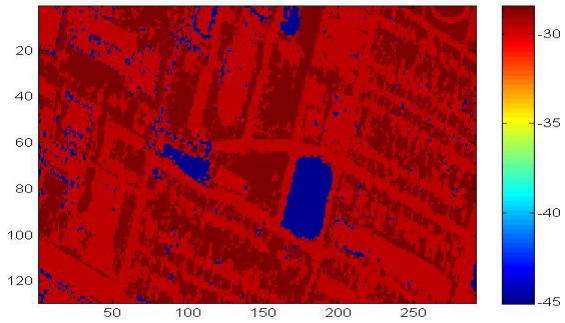

Figure 6. X-band radar clutter map.

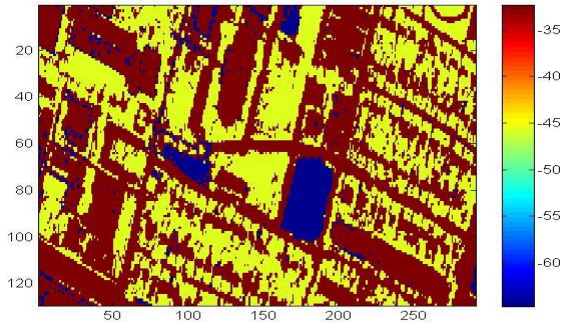

Figure 6. VHF-band radar clutter map.

ACKNOWLEDGMENT

The authors would like to thank the Hyperspectral Image Analysis group and the NSF Funded Center for Airborne Laser Mapping (NCALM) at the University of Houston for providing the data sets used in this study, and the IEEE GRSS Data Fusion Technical Committee for organizing the 2013 Data Fusion Contest.

REFERENCES

[1] De Maio, A., Farina, A., Foglia, G., "Knowledge-based recursve least squares techniques for heterogeneous clutter suppression," IET Radar, Sonar and Navigation, Vol. 1, Issue 2, pp. 106-115, 2007.

[2] Garside, J.R., Oliver, C.J., "A comparison of clutter texture properties in optical and SAR images," in Proc. IEEE International Geoscience and Remote Sensing Symposium (IGARSS), Edinburgh, Scotland, 13-16 Sept. 1988.

[3] Darrah, C.A., Luke, D.W., "Site-specific clutter modeling using DMA digital terrain elevation data (DTED), digital feature analysis data (DFAD), and Lincoln Laboratory five frequency clutter amplitude data," in Proc. IEEE National Radar Conference, Ann Arbor, Michigan, 13-16 May, 1996.

[4] Billingsley, J.B., Larrabee, "Multifrequency measurements of radar ground clutter at 42 sites," MIT Lincoln Laboratory Technical Report 916, Vol. 1, ESD-TR-91-061, 15 November 1991.

[5] Cobo, B., Valle, L., Torres, R.P., "A site-specific radar simulator for clutter modeling in VTS systems," in Proc. 50th International Symposium ELMAR, Zadar, Croatia, 10-12 September, 2008.

[6] Jylha, J., Kerminen, R., Vihonen, J., Ala-Kleemola, T., Visa, A., "New aspects to knowledge-aided clutter analysis," in Proc. IEEE Radar Conference, Verona, NY, April 2006.

[7] Rode, G., "Radar clutter backscattering simulation for specific sites," Frequenz. Volume 62, Issue 1-2, Pages 7–11, February 2008.

[8] Wang, A., Zhang, W., Cao, J., "Terrain clutter modeling for airborne radar system using digital elevation model," in Proc. International Workshop on Microwave and Millimeter Wave Circuits and System Technology (MMWCST), 19-20 April, 2012.

[9] Shasha, L., "Simulation of the radar ground clutter based on DEM," IJCSI International Journal of Computer Science Issues, Vol. 10, Issue 3, No 1, May 2013.

[10] Lin, C.C., Reilly, J.P., "A site-specific model of radar terrain backscatter and shadowing," John Hopkins APL Technical Digest, Vol. 18, pp. 432-447, 1997.

[11] Kurekin, A., Radford, D., Lever, K., Marshall, D., Shark, L.K., "New method for generating site-specific clutter map for land-based radar by using multimodal remote-sensing images and digital terrain data," IET Radar, Sonar, and Navigation, Vol. 5, Iss. 3, pp. 374-388, 2011.

[12] Richards, M.A., Scheer, J.A., Holm, W.A. (ed.), Principles of Modern Radar: Basic Principles (Vol. 1), SciTech Publishers, 2010.

[13] Billingsley, J.B., Low Angle Radar Land Clutter, SciTech Pub., 1991.

[14] Mahafza, R., Radar Systems Analysis and Design Using MATLAB, Chapman and Hall/CRC Press, 2000.

[15] Dong, Y., "Models of land clutter vs grazing angle, spatial distribution and temporal distribution - L-band VV polarization perspective," Australian Dept. of Defense, Defense Science and Technology Organization, Report DSTO-RR-0273, 2004.

[16] Kulemin, G.P., Millimeter Wave Radar Targets and Clutter, Artech House, Norwood, MA, 2003.

[17] Boucard, H. Gach, T., Sicsik-Pare, E. "CRECUS: A radar sensor for battlefield surveillance UAVs," in *Proc. Of RTO SCI Symposium on "Warfare Automation: Procedures and Techniques for Unmanned Vehicles,"* Ankara, Turkey, 26-28 April 1999.

[18] Schwartz, C.E., Bryant, T.G., Cosgrove, J.H., Morse, G.B., and Noonan, J.K., "A radar for unmanned air vehicles," *Lincoln Lab Journal*, Vol. 3, No. 1, 1990.